Diagnostic Accuracy Study

Medicine®

OPEN

Liver lobe based intravoxel incoherent motion diffusion weighted imaging in hepatitis B related cirrhosis: Association with child-pugh class and esophageal and gastric fundic varices

Fan Chen, MS[a,b], Yan-li Chen, MS[a,b], Tian-wu Chen, MD[a,*], Rui Li, MD[a,*], Yu Pu, MS[a], Xiao-ming Zhang, MD[a], Hong-jun Li, MD[c], Sun Tang, MS[a], Jin-ming Cao, MS[a], Jian-qiong Yang, MS[a]

Abstract

Liver cirrhosis is a common chronic progressive liver disease in clinical practice, and intravoxel incoherent motion (IVIM) is a promising magnetic resonance method to assess liver cirrhosis, so our purpose was to investigate association of liver-lobe-based IVIM-derived parameters with hepatitis-B-related cirrhosis and its severity, and esophageal and gastric fundic varices. Seventy-four patients with hepatitis-B-related cirrhotic and 25 healthy volunteers were enrolled and underwent upper abdominal IVIM diffusion-weighted imaging with *b*-values of 0, 20, 50, 80, 100, 200, 400, 600, and 800 s/mm^2. IVIM-derived parameters (*D*, pure molecular diffusion; D^*, pseudo diffusion; and *f*, perfusion fraction) of left lateral lobe (LLL), left medial lobe (LML), right lobe (RL), and caudate lobe (CL) were assessed statistically to show their associations with cirrhosis and its severity, and esophageal and gastric fundic varices. In this research, we found that *D*, D^*, and *f* values of LLL, LML, RL, and CL were lower in cirrhotic liver than in normal liver (all *P*-values $<.05$). *D*, D^*, and *f* values of LLL, LML, RL, and CL were inversely correlated with Child–Pugh class of cirrhosis ($r=-0.236$ to -0.606, all *P*-values $<.05$). *D* of each liver lobe, D^* of LLL and CL, and *f* of LLL, LML, and CL in patients with esophageal and gastric fundic varices were lower than without the varices (all *P*-values $<.05$). *D* values of RL and CL could best identify cirrhosis, and identify esophageal and gastric fundic varices with areas under receiver-operating characteristic curve of 0.857 and 0.746, respectively. We concluded that liver-lobe-based IVIM-derived parameters can be associated with cirrhosis, and esophageal and gastric fundic varices.

Abbreviations: AASLD = American Association for the Study of Liver Diseases, AUC = area under the ROC curve, CL = caudate lobe, *D* = true diffusion coefficient, D^* = pseudo-diffusion coefficient, DWI = diffusion weighted imaging, *f* = perfusion fraction, FOV = field of view, ICC = intraclass correlation coefficient, IVIM = intravoxel incoherent motion, LAVA = liver acquisition with volume acceleration, LLL = left lateral lobe, LML = left medial lobe, MR = magnetic resonance, NSA = number of signal average, RL = right lobe, ROC = receiver-operating characteristic, ROI = region of interest, TE = echo time, TR = repetition time.

Keywords: magnetic resonance imaging, diffusion magnetic resonance imaging, liver, cirrhosis, esophageal and gastric fundic varices

1. Introduction

Liver cirrhosis is a common chronic progressive liver disease in clinical practice. Quantitative evaluation of liver cirrhosis and its severity is of great importance for choosing appropriate clinical interventions. Early cirrhotic liver often reserve good liver function, and etiologic treatment is needed; but when it progresses, more complications (such as bleeding of esophageal and gastric fundic varices, ascites, and hepatic encephalopathy) would happen and it is crucial to take appropriate measures to

Editor: Undurti N. Das.

FC, YC, and YP authors contributed equally to the work.

This study was supported by the Nanchong-University Cooperative Research Project (grant no: NSMC20170206).

The authors have no funding and conflicts of interest to disclose.

[a] Sichuan Key Laboratory of Medical Imaging, and Department of Radiology, Affiliated Hospital of North Sichuan Medical College, Nanchong, Sichuan, [b] Department of Radiology, Southwest Hospital, Army Medical University (Third Military Medical University), Chongqing, [c] Department of Radiology, Beijing YouAn Hospital, Capital Medical University, Beijing, China.

[*] Correspondence: Tian-wu Chen, Rui Li, Sichuan Key Laboratory of Medical Imaging, and Department of Radiology, Affiliated Hospital of North Sichuan Medical College, 63# Wenhua Road, Nanchong 637000, Sichuan, China (e-mails: tianwuchen_nsmc@163.com, dtwg_nsmc@163.com).

How to cite this article: Chen F, Chen Yl, Chen Tw, Li R, Pu Y, Zhang Xm, Li Hj, Tang S, Cao Jm, Yang Jq. Liver-lobe-based intravoxel incoherent motion diffusion weighted imaging in hepatitis-B-related cirrhosis: association with Child–Pugh class and esophageal and gastric fundic varices. Medicine 2020;99:2(e18671).

Received: 20 May 2019 / Received in final form: 23 September 2019 / Accepted: 6 December 2019

http://dx.doi.org/10.1097/MD.0000000000018671

improve patients' survival quality.[1] Clinically, the severity of liver cirrhosis is commonly assessed by the symptom and biochemical blood indicators. As known to all, the Child–Pugh classification is a method used widely to assess the severity of cirrhosis with the combination of biochemical indicators. According to the Child–Pugh scoring system, liver cirrhosis can be classified as 3 grades: low (class A), intermediate (class B), and poor (class C) risk.[1] In addition, esophageal and gastric fundic varices are common complications secondary to portal hypertension in cirrhosis, and have a high risk of causing life-threatening upper gastrointestinal hemorrhage.[2] Endoscopy is the gold standard for the identification of the varices.[3] Nevertheless, endoscopy is invasive and repeated endoscopic examination may lead discomfort for patients. Thus, a noninvasive and repeatable method is needed to demonstrate esophageal and gastric fundic varices.

Magnetic resonance (MR) imaging is promising for assessing liver cirrhosis with the advantages of noninvasion and repeatability.[4] Meanwhile, a variety of MR techniques such as T_1 or T_1 rho mapping, dynamic contrast-enhanced MR imaging, MR elastography, and diffusion-weighted imaging (DWI) have been used to evaluate the severity of liver cirrhosis.[5–8] Initially developed by Le Bihan et al,[9] intravoxel incoherent motion (IVIM) DWI is a promising method to assess liver cirrhosis for its potential to multiparametric imaging with combined effects of diffusion and perfusion. It could detect the changes of diffusion and perfusion in vivo by measuring the true diffusion coefficient (D), pseudo-diffusion coefficient (D^*), and perfusion fraction (f). Liver cirrhosis is associated with abnormal accumulation of extracellular collagen, which may affect both the true diffusion and microcirculation. Currently, many researches have already proved the effects of diffusion and perfusion in the process of liver cirrhosis by using IVIM.[10–14] However, there were few researches on the severity of liver cirrhosis and esophageal and gastric fundic varices by using IVIM.

Commonly, hypertrophy of the left lateral lobe (LLL) and caudate lobe (CL), and atrophy of the left medial lobe (LML) and right lobe (RL) at the same time would occur as the normal liver progresses into cirrhotic liver.[15] We want to know which liver-lobe-based IVIM-derived parameters could be best associated with cirrhosis and its severity, and esophageal and gastric fundic varices. To the best of our knowledge, there are no reports focusing on the liver-lobe-based IVIM-derived parameters to assess the severity and the varices secondary to hepatitis-B-related cirrhosis. Thus, the aim of this study was to explore the association of liver-lobe-based parameters derived from DWI using IVIM with hepatitis-B-related cirrhosis and its severity, and esophageal and gastric fundic varices.

2. Materials and methods

2.1. Patients

The prospective study was approved by the institutional ethics review board of our hospital, and a written informed consent was obtained from each participant prior to the study.

From April 2016 to December 2017, 80 consecutive patients with liver cirrhosis underwent abdominal MR imaging were enrolled in this research referred to the inclusion criteria: hepatitis-B-related liver cirrhosis was confirmed by the laboratory investigations, pathologic findings, and medical imaging according to the American Association for the Study of Liver Diseases (AASLD) practice guidelines on chronic hepatitis B (2018)[16]; patients underwent the test on the 5 parameters including albumin, ascites, bilirubin, prothrombin activity, and encephalopathy to calculate the Child–Pugh score; and patients had no hepatic carcinoma, or other malignant or benign tumors (except for liver cyst) shown on the MR imaging. The exclusion criteria were as follows: prohibitions for MR scan; patients with hepatic carcinoma (n = 1) or portal vein emboli (n = 2); patients with active bleeding in gastrointestinal tract (n = 1); patients with history of treatment for portal hypertension (such as splenectomy, splenic artery embolization [n = 1], transjugular intrahepatic portosystemic shunt); patients with chronic severe renal impairment (n = 1); or patients with a poor coordination of respiratory.

Based on the clinical, biologic, endoscopic, and MR data, 74 cases with liver cirrhosis were enrolled in this study. In this cohort, there were 45 males and 29 females in the cirrhotic group with mean age of 48.8 years (range, 20–79 years). According to the Child–Pugh scoring system, 28, 24, and 22 patients were classified as Child–Pugh class A, B, and C, respectively. The Child–Pugh score was calculated within 3 days before or after the MR scanning. The endoscopy was used to demonstrate esophageal and gastric fundic varices. In this cohort, 30 patients had esophageal and gastric fundic varices and 44 patients did not have the varices.

During the same research period, 25 consecutive healthy volunteers including 11 males and 14 females with mean age of 45.3 years (range, 21–50 years) who underwent upper abdominal IVIM DWI were randomly enrolled in this cohort as the control group. The inclusion criteria for the control group were listed as follows: the participants had no history of chronic viral infection, alcohol abuse and liver surgery, and currently did not receive medical treatment; hepatitis virus markers were negative and liver function was normal based on the laboratory examination; and there were no MR findings of chronic liver disease, hepatic carcinoma, or fatty liver.

2.2. MR technique

A 3.0-T scanner (Discovery MR 750; GE Medical Systems, Milwaukee, Wis, USA), equipped with 32 channel body coil, was used to perform the upper abdominal MR examination when the respiratory signals were established. All subjects were required fasting more than 4 hours before the examination. The MR sequences included T_1-weighted axial liver acquisition with volume acceleration (LAVA) Flex mask, fat-suppressed axial T_2-weighted sequence, and axial IVIM sequence followed by the contrast-enhanced LAVA sequences. The scanning parameters for the above mentioned sequences were as follows: repetition time (TR) of 3.7 milliseconds, echo time (TE) of 1.8 milliseconds, matrix of 128×128, field of view (FOV) of $340\,mm \times 340\,mm$, slice thickness of 5.2 mm, number of signal average (NSA) of 1, and bandwidth of 200 kHz for T_1-weighted axial LAVA-Flex mask; TR of 3750 milliseconds, TE of 96 milliseconds, matrix of 320×320, FOV of $340\,mm \times 340\,mm$, slice thickness of 5 mm, slice gap of 1 mm, NSA of 2, and bandwidth of 83.33 kHz for T_2-weighted imaging; and TR of 1500 milliseconds, TE of 63 milliseconds, matrix of 256×256, FOV of $360\,mm \times 360\,mm$, slice thickness of 5 mm, slice gap of 1 mm, b value of 0, 20, 50, 80, 100, 200, 400, 600, and $800\,s/mm^2$, and NSA of 1 for IVIM DWI. Subsequently, each patient with liver cirrhosis was injected

gadodiamide (Magnevist; Bayer Healthcare, Germany) with a standard dose of 0.2 mmol/kg of body weight at a standard flow rate of 3 mL/s through a peripheral venous access followed by a 20-mL saline solution flush for axial contrast-enhanced LAVA acquisitions. In addition, T_1-weighted imaging, T_2-weighted imaging, and contrast-enhanced MR sequences were conducted to determine whether the participants in this cohort were compliant to the inclusion criteria.

2.3. Image analysis

The original IVIM data were directly loaded to the workstation (GE Advanced Workstation version 4.4-09) and a standard software package was used to analyze the IVIM DWI data. This software allowed the calculation of the D, D^*, and f values and the corresponding parametric maps. According to the IVIM principle, the relation between signal intensity and b value complies with the following formula: $S_b/S_0 = f \times \exp(-b \cdot D^*) + (1 - f) \times \exp(-b \cdot D)$, where S_0 represents the signal intensity at the b value of 0 s/mm^2, S_b represents the signal intensity at the given b value, f is the perfusion fraction, D is the diffusion coefficient related to pure molecular diffusion, and D^* is the pseudo diffusion coefficient associated with the microcirculation. Two radiologists (the 1st author with 4-year experience in radiology, and the corresponding author with 21-year experience in abdominal radiology) who were blinded to the clinical, laboratory, and pathologic data, independently performed the analysis of the image data.

The previous data analysis in the liver were based on the 4 liver lobes: LLL, LML, RL, and CL. On the basis of T_2-weighted imaging data, 3 freehand regions of interest (ROIs) were placed on one sectional representative IVIM image in a liver lobe (Fig. 1A). The software automatically calculated the D, D^*, and f values, and the same ROIs were copied to the color coded maps of D (Fig. 1B), D^* (Fig. 1C), and f (Fig. 1D) during the previous analysis. The above-mentioned analysis was repeated on the consecutive other 2 representative sections of the corresponding liver lobe. A total of 9 ROIs in each liver lobe per participant were drawn. The area of each ROI within LLL, LML, and RL was 100 to 150 mm^2 and that in CL was 30 to 50 mm^2. We drew each ROI in each liver lobe by avoiding the areas of artifact, vessels, bile ducts, and intestinal gas. An average of the IVIM-derived parameters across the 9 ROIs in each liver lobe was calculated to serve as the liver-lobe-based parameters.

To test the intraobserver reproducibility of measurements of the liver-lobe-based IVIM-derived parameters, all IVIM DWI were repeatedly analyzed by the 1st author 2 weeks later.

2.4. Statistical analysis

The SPSS package version 13.0 was used for the statistical analysis, and a P-value $<.05$ was considered significantly

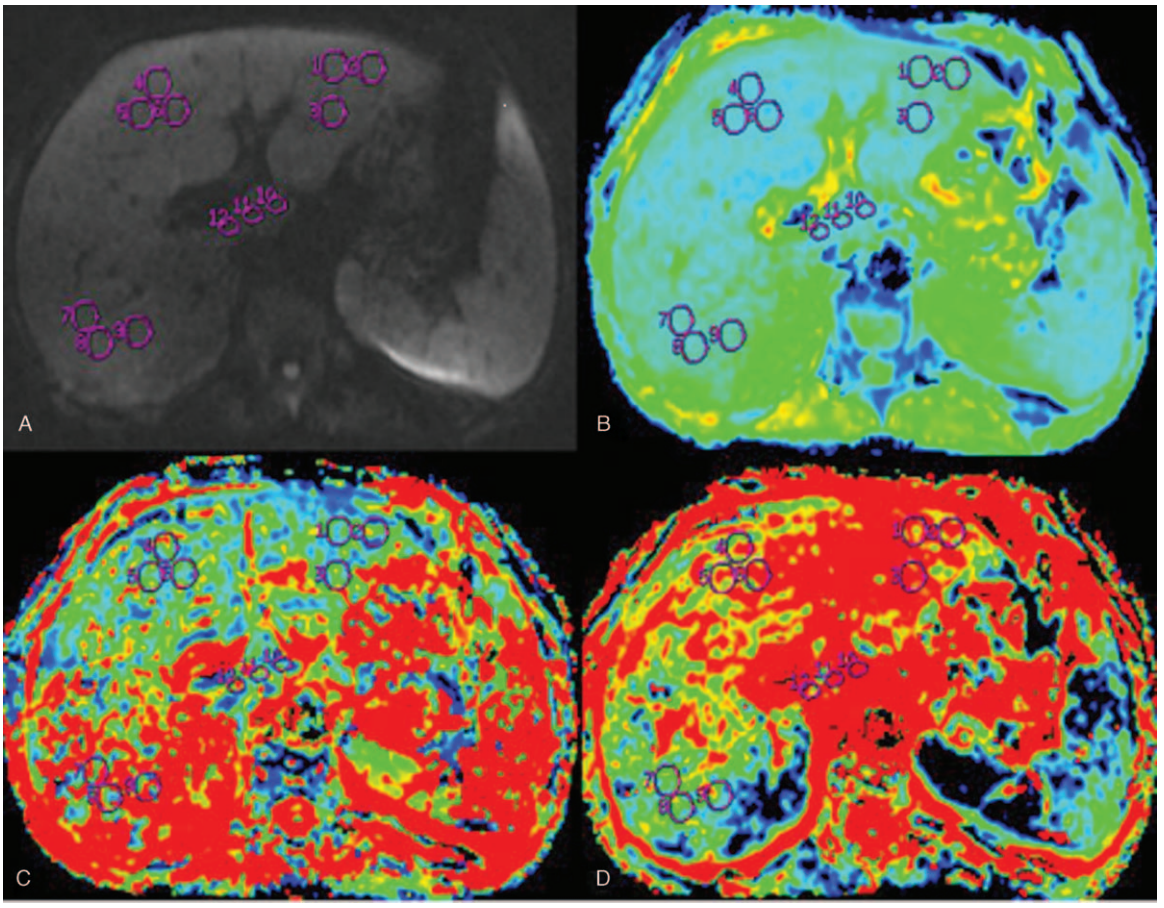

Figure 1. In a 50-year-old male with liver cirrhosis of Child–Pugh class C, 3 regions of interest are randomly drawn each in the left lateral liver lobe, left medial liver lobe, right liver lobe, and caudate lobe on diffusion weighted imaging using b value of 0 s/mm^2 (A) to obtain the intravoxel incoherent-motion-derived parameters. The regions of interest are identically positioned in the corresponding parametric maps of the D (B), D^* (C), and f (D) by the postprocessing software.

Table 1

Reproducibility of the intravoxel incoherent-motion-derived parameters' measurements in the enrolled participants.

	Interobserver		Intraobserver	
	ICC	95% CI	ICC	95% CI
D ($\times 10^{-3}$ mm^2/s)				
LLL	0.979	0.969–0.986	0.971	0.957–0.981
LML	0.985	0.978–0.989	0.964	0.947–0.976
RL	0.954	0.932–0.969	0.990	0.985–0.993
CL	0.966	0.950–0.977	0.989	0.984–0.993
D^* ($\times 10^{-3}$ mm^2/s)				
LLL	0.955	0.933–0.969	0.943	0.916–0.961
LML	0.920	0.884–0.946	0.958	0.939–0.972
RL	0.925	0.891–0.949	0.948	0.923–0.965
CL	0.926	0.892–0.950	0.994	0.991–0.996
f				
LLL	0.916	0.878–0.943	0.922	0.886–0.947
LML	0.905	0.862–0.935	0.900	0.855–0.932
RL	0.904	0.861–0.935	0.969	0.953–0.979
CL	0.911	0.870–0.939	0.968	0.952–0.978

95% CI = 95% confidence interval, CL = caudate lobe, ICC = interclass coefficient, LLL = left lateral lobe of the liver, LML = left medial lobe of the liver, RL = right lobe of the liver.

different. Descriptive statistics for liver-lobe-based IVIM-derived parameters were expressed as mean ± standard deviation. Kruskal–Wallis test was used to compare the liver-lobe-based IVIM-derived parameters between the cirrhotic and control groups. And the Student t test was used to compare the previous IVIM-derived parameters between patients with and without esophageal and gastric fundic varices. The correlation between each liver-lobe-based IVIM-derived parameter and Child–Pugh class was assessed by Spearman rank correlation analysis. Receiver-operating characteristic (ROC) curve was generated to evaluate the diagnostic performance of any liver-lobe-based IVIM-derived parameter for identifying liver cirrhosis, and esophageal and gastric fundic varices with a quantitative index (the area under the ROC curve, AUC).

In addition, to determine the reproducibility of the measurements of liver-lobe-based IVIM-derived parameters, the interobserver and intraobserver intraclass correlation coefficients (ICCs) were calculated. When the ICC was >75%, the reproducibility of the liver-lobe-based IVIM-derived parameter measurements was regarded sufficient, and an average of the 2 authors' 1st measurement was used as the final results to perform the subsequent analysis. When the ICC was <75%, 2 additional measurements were performed by the above-mentioned 2 authors, and an average of the 4 measurements was used as the final value.

3. Results

3.1. Inter- and intraobserver reproducibility of liver-lobe-based IVIM-derived parameter measurement

In this study, the 1st measurements of both observers were used to evaluate the interobserver reproducibility. The 2 measurements from the 1st author were used to analyze the intraobserver reproducibility. The ICCs on the inter- or intraobserver reproducibility of liver-lobe-based IVIM-derived parameter measurements are shown in Table 1. The ICCs for the inter- and intraobserver reproducibility were more than 0.9, which indicated that the reproducibility of the measurements was very good. Therefore, we used the average of the first measurements from the 2 authors as the final results for the subsequent analysis.

3.2. Evaluation of cirrhosis and its Child–Pugh class with liver-lobe-based IVIM-derived parameters

The liver-lobe-based IVIM-derived parameters in the cirrhotic group and the control group are shown in Table 2 and Figure 2. According to the Kruskal–Wallis test, the D, D^*, and f values of each liver lobe in the cirrhotic group were lower than in the control group (all P-values <.05). Spearman rank correlation analysis showed that the D, D^*, and f values of each liver lobe were negatively correlated with the Child–Pugh class, as shown in Table 3 (all P-values <.05).

Table 2

Pure molecular diffusion (D), pseudo-diffusion coefficient (D^*), and perfusion fraction (f) values in healthy volunteers and patients with cirrhosis.

	Healthy volunteer	Cirrhotic patient	Child–Pugh class of cirrhosis		
	(n = 25)	(n = 74)	A (n = 28)	B (n = 24)	C (n = 22)
D ($\times 10^{-3}$ mm^2/s)					
LLL	1.144 ± 0.192	0.886 ± 0.181†	0.964 ± 0.192	0.883 ± 0.172	0.791 ± 0.131
LML	1.161 ± 0.196	0.892 ± 0.173†	0.973 ± 0.164	0.905 ± 0.146	0.777 ± 0.152
RL	1.167 ± 0.203	0.871 ± 0.168†	0.936 ± 0.160	0.886 ± 0.149	0.770 ± 0.158
CL	1.108 ± 0.215	0.893 ± 0.176†	0.958 ± 0.171	0.895 ± 0.155	0.810 ± 0.176
D^* ($\times 10^{-3}$ mm^2/s)					
LLL	64.364 ± 20.045	49.521 ± 15.387†	51.102 ± 14.514	49.402 ± 16.916	47.638 ± 15.222
LML	62.658 ± 18.159	47.999 ± 16.859†	48.817 ± 16.505	47.993 ± 19.529	46.964 ± 14.769
RL	61.825 ± 20.865	46.378 ± 17.229†	49.858 ± 18.263	45.241 ± 17.605	43.190 ± 15.343
CL	63.282 ± 19.245	48.269 ± 19.067†	50.500 ± 23.068	49.617 ± 18.596	43.961 ± 13.146
f					
LLL	0.391 ± 0.133	0.277 ± 0.122†	0.294 ± 0.138	0.276 ± 0.119	0.257 ± 0.134
LML	0.386 ± 0.129	0.266 ± 0.106†	0.287 ± 0.111	0.262 ± 0.105	0.244 ± 0.100
RL	0.371 ± 0.127	0.269 ± 0.112†	0.258 ± 0.123	0.283 ± 0.101	0.266 ± 0.114
CL	0.368 ± 0.122	0.258 ± 0.113†	0.279 ± 0.109	0.255 ± 0.120	0.235 ± 0.109

All data are expressed as mean ± standard deviation.

CL = caudate lobe, LLL = left lateral lobe of the liver, LML = left medial lobe of the liver, RL = right lobe of the liver.

† A significant difference in the intravoxel incoherent-motion-derived parameter between cirrhotic patients and healthy volunteers (P< .05).

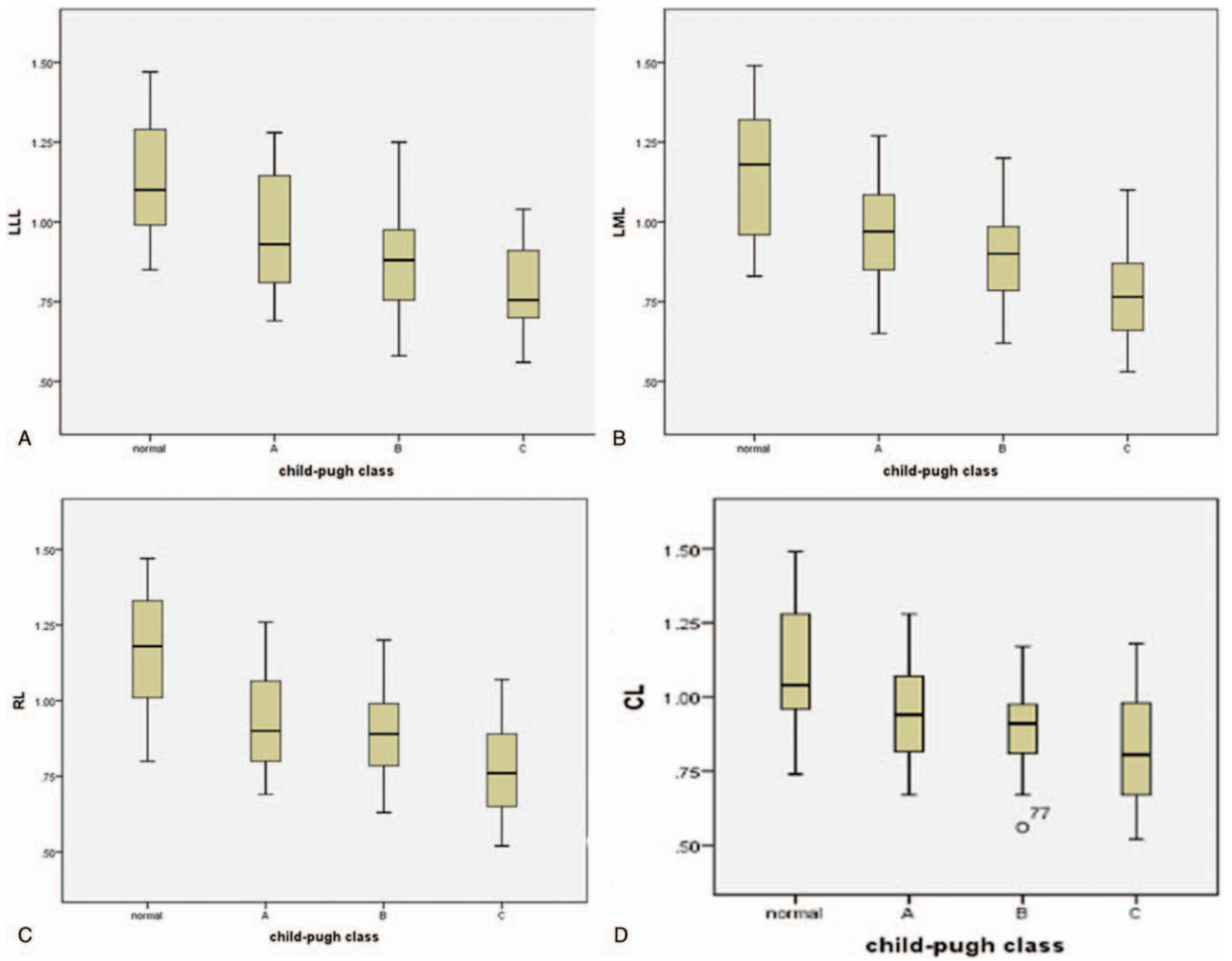

Figure 2. Box plots show the *D* values of left lateral liver lobe (LLL, A), left medial liver lobe (LML, B), right liver lobe (RL, C), and caudate lobe (CL, D) in normal participants and patients with cirrhosis of different Child–Pugh classes.

Table 3

Association of the liver-lobe-based intravoxel incoherent-motion-derived parameters with the Child–Pugh class of liver cirrhosis.

	Correlation index (*r*)	*P*-value
D ($\times 10^{-3}$ mm^2/s)		
LLL	−0.582	<.001
LML	−0.606	<.001
RL	−0.589	<.001
CL	−0.471	<.001
D^* ($\times 10^{-3}$ mm^2/s)		
LLL	−0.305	.002
LML	−0.275	.006
RL	−0.316	.001
CL	−0.326	.001
f		
LLL	−0.333	.001
LML	−0.374	<.001
RL	−0.236	.019
CL	−0.350	<.001

CL = caudate lobe, LLL = left lateral lobe of the liver, LML = left medial lobe of the liver, RL = right lobe of the liver.

3.3. Comparisons of liver-lobe-based IVIM-derived parameters in cirrhotic patients with vs without esophageal and gastric fundic varices

We compared the liver-lobe-based IVIM-derived parameters between cirrhotic patients with and without esophageal and gastric fundic varices, which is illustrated in Table 4. According to the 2 independent samples tests, the *D* values of each liver lobe, the D^* values of LLL and CL, and the *f* values of LLL, LML and CL were lower in patients with esophageal and gastric fundic varices than without the varices (all *P*-values <.05).

3.4. ROC analysis of liver-lobe-based IVIM-derived parameters for determining cirrhosis, and esophageal and gastric fundic varices

The results of the ROC analysis about the determination of cirrhosis, and esophageal and gastric fundic varices with liver-lobe-based IVIM-derived parameters are shown in Table 5 and Figure 3. The *D* value of RL had the highest diagnostic efficiency on the discrimination of cirrhotic liver from normal liver with an

Table 4

Comparisons of the liver-lobe-based intravoxel incoherent-motion-derived parameters between patients with and without esophageal and gastric fundic varices.

	Esophageal and gastric fundic varices		
	No (n = 44)	Yes (n = 30)	*P*-value
D ($\times 10^{-3}$ mm^2/s)			
LLL	0.941 ± 0.182	0.805 ± 0.149	.001
LML	0.948 ± 0.155	0.811 ± 0.167	<.001
RL	0.927 ± 0.152	0.789 ± 0.158	<.001
CL	0.951 ± 0.164	0.808 ± 0.160	<.001
D^* ($\times 10^{-3}$ mm^2/s)			
LLL	52.882 ± 15.200	44.591 ± 14.528	.021
LML	50.957 ± 17.300	43.661 ± 15.458	.062
RL	48.917 ± 17.103	42.654 ± 17.013	.126
CL	52.123 ± 20.493	42.618 ± 15.394	.026
f			
LLL	0.303 ± 0.128	0.241 ± 0.105	.027
LML	0.293 ± 0.109	0.226 ± 0.089	.005
RL	0.289 ± 0.117	0.238 ± 0.099	.051
CL	0.285 ± 0.111	0.219 ± 0.104	.012

CL = caudate lobe, LLL = left lateral lobe of the liver, LML = left medial lobe of the liver, RL = right lobe of the liver.

AUC of 0.857. In addition, the D value of CL could best identify esophageal and gastric fundic varices with an AUC of 0.746.

4. Discussion

In this study, we used liver-lobe-based IVIM-derived parameters to investigate the identification of cirrhosis and esophageal and gastric fundic varices. We found that the D, D^*, and f values of each liver lobe in the cirrhotic patients decreased significantly in comparison with the healthy participants, and were inversely correlated with the Child–Pugh class of cirrhosis. The reason for the decreasing trend of D value in liver cirrhosis was closely related to the pathologic mechanism. On one hand, with the progression of the liver cirrhosis, collagen fibers continuously generate and deposit in the extracellular Disse space, which leads to the narrowing of extracellular and then restricting the diffusion of water molecular. On the other hand, the content of external water molecular would reduce along with the increase of collagen fibers in cirrhotic liver, which may lead to the decrease of D value.[17–19]

As shown in our study, D^* and f values of cirrhotic liver also decreased when compared to healthy liver, which would account to the reduced perfusion during the process of liver cirrhosis. With the progression of cirrhosis, the narrowed extracellular space will compress the portal vein, which leads to the increase of the resistance in the portal vein, eventually resulting in the formation of portal hypertension and the decrease of portal blood flow. Since the primary blood supply of the liver comes from portal vein and the supply of hepatic artery cannot compensate the reduced portal flow in cirrhotic liver, the perfusion of the whole liver would decrease.[20,21] However, some researches had different conclusions. Luciani et al[10] and Chow et al[22] reported that the D^* value decreased significantly in cirrhotic liver while f value had no difference between cirrhotic and healthy liver. In an experimental study,[20] Zhang et al reported that f value decreased significantly in cirrhotic liver while D^* value did not when compared to healthy liver. We acknowledged that different studies may have discrepancies on the results of D^* or f value in cirrhotic liver, but they all indicated the reduction of perfusion in the process of liver cirrhosis.

The ROC analysis in our study showed that the D value of each liver lobe had higher diagnostic performance for the identification of liver cirrhosis than f or D^* values. Among the 4 liver lobes, the D value of RL had the highest diagnostic performance than those of LLL, LML, and CL (AUC: 0.857 vs 0.837, 0.835, and 0.778, respectively). The reason why the D value had a higher diagnostic performance than f and D^* values may be explained by the accuracy of the measurements of the IVIM-derived parameters, which were influenced by many factors including the setting of b value (especially on the number of b value <200 s/

Table 5

Receiver-operating characteristic analysis of the liver-lobe-based intravoxel incoherent-motion-derived parameters for determining cirrhosis and esophageal and gastric fundic varices.

	Cut-off value	Group	AUC	Sensitivity	Specificity
D ($\times 10^{-3}$ mm^2/s)					
LLL	0.97	Normal vs cirrhosis	0.837	0.8	0.73
	0.84	Cirrhosis: no varices vs varices	0.723	0.73	0.63
LML	1.08	Normal vs cirrhosis	0.835	0.72	0.85
	0.87	Cirrhosis: no varices vs varices	0.736	0.68	0.73
RL	1.11	Normal vs cirrhosis	0.857	0.68	0.93
	0.78	Cirrhosis: no varices vs varices	0.738	0.84	0.57
CL	0.94	Normal vs cirrhosis	0.778	0.84	0.64
	0.80	Cirrhosis: no varices vs varices	0.746	0.86	0.5
D^* ($\times 10^{-3}$ mm^2/s)					
LLL	54.87	Normal vs cirrhosis	0.725	0.76	0.62
LML	53.64	Normal vs cirrhosis	0.716	0.72	0.61
RL	57.19	Normal vs cirrhosis	0.702	0.7	0.6
CL	46.85	Normal vs cirrhosis	0.711	0.84	0.51
f					
LLL	0.42	Normal vs cirrhosis	0.737	0.52	0.86
LML	0.38	Normal vs cirrhosis	0.751	0.56	0.88
RL	0.27	Normal vs cirrhosis	0.724	0.84	0.54
CL	0.37	Normal vs cirrhosis	0.734	0.52	0.87

AUC = area under the receiver-operating characteristic curve, CL = caudate lobe, LLL = left lateral lobe of the liver, LML = left medial lobe of the liver, RL = right lobe of the liver.

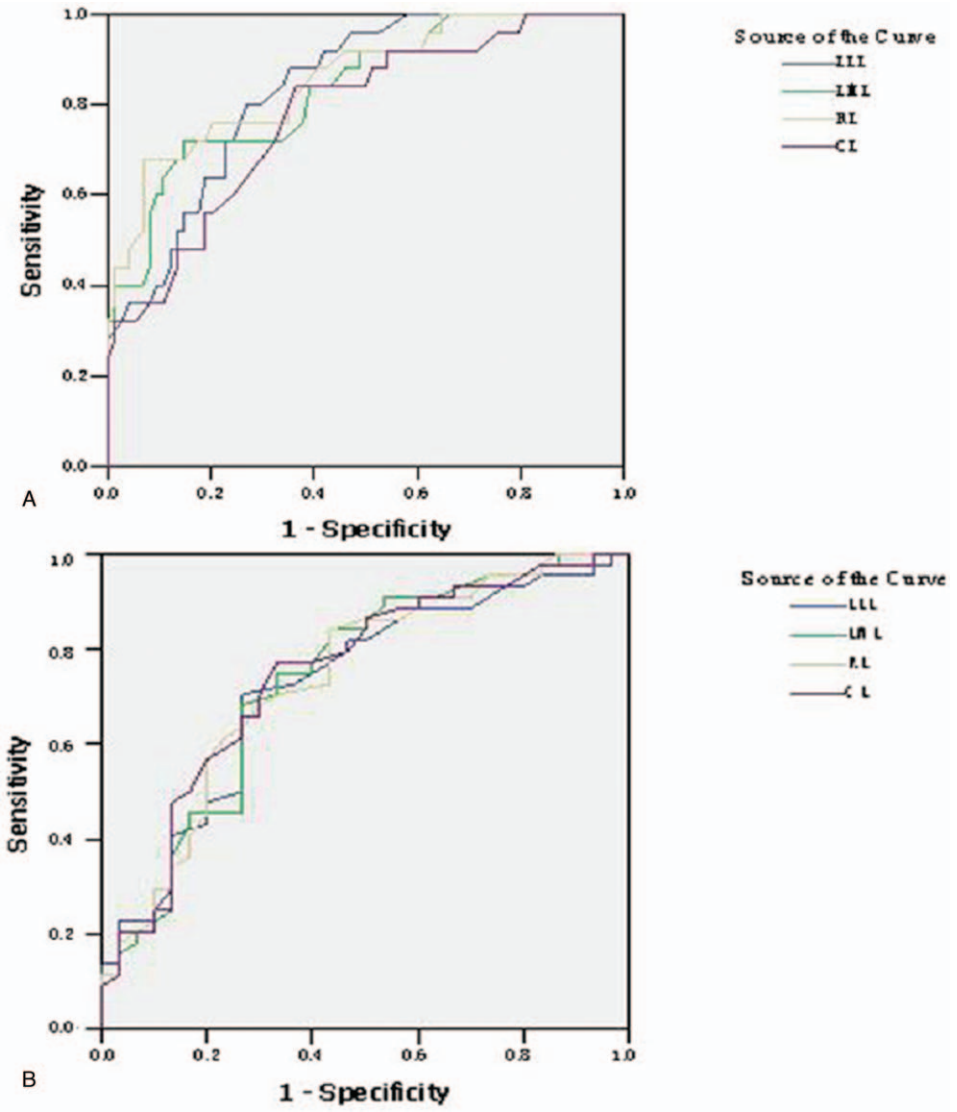

Figure 3. Receiver-operating characteristic analyses of liver-lobe-based parameters derived from intravoxel incoherent motion are performed to identify cirrhosis, and esophageal and gastric fundic varices. The receiver-operating characteristic curves show that the *D* value of left lateral liver lobe (LLL), left medial liver lobe (LML), right liver lobe (RL), and caudate lobe (CL) could be indicators for the identification of cirrhosis (A), and cirrhotic patients between with and without esophageal and gastric fundic varices (B).

mm^2), and the interference of breath and heart artifact.[23–28] The D^* and *f* values were easily affected by the setting of lower *b* value. In this study, there were fewer *b* values <200 s/mm^2, which may influence the accuracy of the measurement of the D^* and *f* values. In addition, LLL of liver is close to the heart and CL is close to the porta hepatis, which is more easily disturbed by the motion artifact of the neighboring organs.

In addition, our study demonstrated that the *D* value of each liver lobe, D^* value of LLL and CL, and *f* value of LLL, LML and CL were lower in liver cirrhosis with esophageal and gastric fundic varices than without the varices. For the first time, the ROC analysis in our study revealed that the *D* value of CL could best identify esophageal and gastric fundic varices with an AUC of 0.746. In comparison with fibroscan to predict the existence of esophageal and gastric fundic varices,[29] liver-lobe-based IVIM-derived parameters do not have better power than Fibroscan (AUC: 0.746 vs 0.8262), suggesting that liver-lobe-based IVIM DWI cannot improve prediction of the varices. We will perform the further study focusing on the combination of the liver-lobe-based IVIM DWI and other MR sequences such as portal venography to improve prediction power.

This study has several limitations. First, not all cases with liver cirrhosis were confirmed by pathology. But the hepatitis-B-related liver cirrhosis in the other patients was confirmed by the laboratory investigations and medical imaging according to the AASLD practice guidelines (2018).[16] Second, the method for assessing the severity of liver function was Child–Pugh classification system, the subjectivity was inevitable in the assessment of Child–Pugh classification. We will perform the future study on the basis of another more objective method to confirm our results. Third, because of small sample sizes corresponding to some of the continuing Child–Pugh scores, we did not make up the correlation tests of the *D*, D^*, and *f* values with the continuing Child–Pugh scores. We will further enlarge

the sample size to investigate the previous correlations. Fourth, we did not describe whether our methods can predict the severity of varices and compare our results with Baveno VI recommendation because the theme of our study was not to assess the risk of having varices requiring treatment but to investigate association of liver-lobe-based IVIM-derived parameters with hepatitis-B-related cirrhosis and esophageal and gastric fundic varices. We will perform the relevant study in the future.

5. Conclusion

Liver-lobe-based IVIM-derived parameters could be used to assess liver cirrhosis and its Child–Pugh class, and identify esophageal and gastric fundic varices. The *D* value of RL had the highest diagnostic performance for the identification of liver cirrhosis, and the *D* value of CL could best identify esophageal and gastric fundic varices. We hope that these findings might be useful to quantitatively evaluate liver cirrhosis as a supplementary means for treatment decision making in clinical settings.

Author contributions

Conceptualization: Fan Chen, Tian-wu Chen, Rui Li, Xiao-ming Zhang, Hong-jun Li.
Data curation: Fan Chen, Yan-li Chen, Sun Tang.
Formal analysis: Fan Chen, Yan-li Chen, Sun Tang.
Funding acquisition: Tian-wu Chen.
Investigation: Fan Chen, Yan-li Chen, Sun Tang, Jin-ming Cao, Jian-qiong Yang.
Methodology: Fan Chen, Yan-li Chen, Tian-wu Chen, Rui Li, Yu Pu, Xiao-ming Zhang, Hong-jun Li, Jin-ming Cao.
Project administration: Tian-wu Chen, Rui Li, Yu Pu, Xiao-ming Zhang, Hong-jun Li.
Resources: Tian-wu Chen, Yu Pu.
Supervision: Tian-wu Chen, Rui Li, Yu Pu, Xiao-ming Zhang, Hong-jun Li.
Validation: Fan Chen, Yan-li Chen, Sun Tang, Jin-ming Cao, Jian-qiong Yang.
Visualization: Fan Chen, Yan-li Chen, Tian-wu Chen, Sun Tang, Jin-ming Cao, Jian-qiong Yang.
Writing – original draft: Fan Chen, Yan-li Chen, Tian-wu Chen, Rui Li, Jian-qiong Yang.
Writing – review & editing: Fan Chen, Tian-wu Chen, Rui Li, Hong-jun Li.
Tian-wu Chen orcid: 0000-0001-5776-3429.

References

[1] Bhat M, Ghali P, Deschenes M, et al. Prevention and management of chronic hepatitis B. Int J Prev Med 2014;5:S200–7.
[2] Biecker E. Portal hypertension and gastrointestinal bleeding: diagnosis, prevention and management. World J Gastroenterol 2013;19:5035–50.
[3] de Franchis R, Baveno VI Faculty . Expanding consensus in portal hypertension: report of the Baveno VI Consensus Workshop: Stratifying risk and individualizing care for portal hypertension. J Hepatol 2015;63:743–52.
[4] Schiavon Lde L, Narciso-Schiavon JL, de Carvalho-Filho RJ. Noninvasive diagnosis of liver fibrosis in chronic hepatitis C. World J Gastroenterol 2014;20:2854–66.
[5] Allkemper T, Sagmeister F, Cicinnati V, et al. Evaluation of fibrotic liver disease with whole liver T1ρ MR imaging: a feasibility study at 1.5 T. Radiology 2014;271:408–15.
[6] Juluru K, Talal AH, Yantiss RK, et al. Diagnostic accuracy of intracellular uptake rates calculated using dynamic Gd-EOB-DTPA enhanced MRI for hepatic fibrosis stage. J Magn Reson Imaging 2017;45:1177–85.
[7] Hennedige TP, Wang G, Leung FP, et al. Magnetic resonance elastography and diffusion weighted imaging in the evaluation of hepatic fibrosis in chronic hepatitis B. Gut Liver 2017;11:401–8.
[8] Shenoy-Bhangle A, Baliyan V, Kordbacheh H, et al. Diffusion weighted magnetic resonance imaging of liver: principles, clinical applications and recent updates. World J Hepatol 2017;9:1081–91.
[9] Le Bihan D, Breton E, Lallemand D, et al. MR imaging of intravoxel incoherent motions: application to diffusion and perfusion in neurologic disorders. Radiology 1986;161:401–7.
[10] Luciani A, Vignaud A, Cavet M, et al. Liver cirrhosis: intravoxel incoherent motion MR imaging-pilot study. Radiology 2008;249:891–9.
[11] Lu PX, Huang H, Yuan J, et al. Decreases in molecular diffusion, perfusion fraction and perfusion-related diffusion in fibrotic livers: a prospective clinical intravoxel incoherent motion MR imaging study. PLoS One 2014;9:e113846.
[12] Wáng YXJ, Deng M, Li YT, et al. A combined use of intravoxel incoherent motion MRI parameters can differentiate early stage hepatitis-B fibrotic livers from healthy livers. SLAS Technol 2018; 23:259–68.
[13] Hu G, Chan Q, Quan X, et al. Intravoxel incoherent motion MRI evaluation for the staging of liver fibrosis in a rat model. J Magn Reson Imaging 2015;42:331–9.
[14] Chen C, Wang B, Shi D, et al. Initial study of biexponential model of intravoxel incoherent motion magnetic resonance imaging in evaluation of the liver fibrosis. Chin Med J (Engl) 2014;127:3082–7.
[15] Awaya H, Mitchell DG, Kamishima T, et al. Cirrhosis: modified-caudate right lobe ratio. Radiology 2002;224:769–74.
[16] Terrault NA, Lok ASF, McMahon BJ, et al. Update on prevention, diagnosis, and treatment of chronic hepatitis B: AASLD 2018 hepatitis B guidance. Hepatology 2018;67:1560–99.
[17] Li YT, Cercueil JP, Yuan J, et al. Liver intravoxel incoherent motion (IVIM) magnetic resonance imaging: a comprehensive review of published data on normal values and applications for fibrosis and tumor evaluation. Quant Imaging Med Surg 2017;7:59–78.
[18] Yoon JH, Lee JM, Baek JH, et al. Evaluation of hepatic fibrosis using intravoxel incoherent motion in diffusion-weighted liver MRI. J Comput Assist Tomogr 2014;38:110–6.
[19] Guiu B, Petit JM, Capitan V, et al. Intravoxel incoherent motion diffusion weighted imaging in nonalcoholic fatty liver disease: a 3.0-T MR study. Radiology 2012;265:96–103.
[20] Zhang Y, Jin N, Deng J, et al. Intra-voxel incoherent motion MRI in rodent model of diethylnitrosamine-induced liver fibrosis. Magn Reson Imaging 2013;31:1017–21.
[21] Lee JT, Liau J, Murphy P, et al. Cross-sectional investigation of correlation between hepatic steatosis and IVIM perfusion on MR imaging. Magn Reson Imaging 2012;30:572–8.
[22] Chow AM, Gao DS, Fan SJ, et al. Liver fibrosis: an intravoxel incoherent motion (IVIM) study. J Magn Reson Imaging 2012;36: 159–67.
[23] Zhang J, Guo Y, Tan X, et al. MRI-based estimation of liver function by intravoxel incoherent motion diffusion-weighted imaging. Magn Reson Imaging 2016;34:1220–5.
[24] Takayama Y, Nishie A, Asayama Y, et al. Image quality and diagnostic performance of free-breathing diffusion-weighted imaging for hepatocellular carcinoma. World J Hepatol 2017;9:657–66.
[25] ter Voert EE, Delso G, Porto M, et al. Intravoxel incoherent motion protocol evaluation and data quality in normal and malignant liver tissue and comparison to the literature. Invest Radiol 2016;51:90–9.
[26] Yuan J, Wong OL, Lo GG, et al. Statistical assessment of bi-exponential diffusion weighted imaging signal characteristics induced by intravoxel incoherent motion in malignant breast tumors. Quant Imaging Med Surg 2016;6:418–29.
[27] Eghtedari M, Ma J, Fox P, et al. Effects of magnetic field strength and b value on the sensitivity and specificity of quantitative breast diffusion weighted MRI. Quant Imaging Med Surg 2016;6:374–80.
[28] Dyvorne H, Jajamovich G, Kakite S, et al. Intravoxel incoherent motion diffusion imaging of the liver: optimal b-value subsampling and impact on parameter precision and reproducibility. Eur J Radiol 2014;83:2109–13.
[29] Pu K, Shi JH, Wang X, et al. Diagnostic accuracy of transient elastography (FibroScan) in detection of esophageal varices in patients with cirrhosis: a meta-analysis. World J Gastroenterol 2017;23:345–56.